Electrochimica Acta 154 (2015) 379–386

Contents lists available at ScienceDirect

Electrochimica Acta

journal homepage: www.elsevier.com/locate/electacta

Rational Design of Ultra-Short Anodic Alumina Nanotubes by Short-Time Pulse Anodization

Ye Wang [a,b], Abel Santos [a,*], Andreas Evdokiou [b,*], Dusan Losic [a,*]

[a] School of Chemical Engineering, The University of Adelaide, Engineering North Building, 5005 Adelaide, Australia
[b] School of Medicine, Discipline of Surgery, The University of Adelaide, Australia

ARTICLE INFO

Article history:
Received 16 November 2014
Received in revised form 9 December 2014
Accepted 9 December 2014
Available online 11 December 2014

Keywords:
anodic aluminum oxide
pulse anodization
anodic alumina nanotube
current density

ABSTRACT

Herein, we report on a rational electrochemical approach based on pulse anodization (PA) of aluminum for the fabrication of ultra-short anodic alumina nanotubes (AANTs) with exquisitely controlled dimensions. AANTs with average length 485 ± 180 nm and outer diameter 90 ± 10 nm were fabricated by PA with 0.3 M sulfuric acid and 10% ethanol. Our findings suggest that extensive Joule's heat generation at the nanopore's base is critical for optimized AANTs' liberation from pulse-anodized anodic aluminum oxide (AAO) nanostructure. The heat evolution results in an enhanced oxygen generation and a rapid voltage recovery during PA. While oxygen generation weakens the conjunction between cells, rapid voltage recovery generates asynchronous inner/outer wall structural modulation, which consequently facilitates structural cleavage of nanotubes along mild anodization/hard anodization (MA/HA) interfaces after acid etching. The understanding of AANTs fabrication mechanism enables us for the first time to fabricate ultra-short AANTs by reducing HA duration down to 1 second and using ethanol for enhancing heat generation. The resulting AANTs with controlled dimensionse and high liberation yield offer new opportunities for advanced applications such as catalysis, template-assisted nanofabrication, optical sensing and drug delivery.

1. Introduction

Aluminum anodization is a well-established nanofabrication technique used to produce a broad range of anodic aluminum oxide (AAO) nanostructures [1,2]. The resulting self-ordered AAO nanostructures have a wide variety of applications in many fields such as sensing, drug delivery, energy storage, medical devices and molecular separation due to their excellent physiochemical properties [3–6]. Another important application of AAO is to be used as a starting material for fabricating other nanotubular structures by template replica technique [7]. AAO template has many unique properties as compared to other hard templates such as controlled pore size/density, high aspect ratio of long-range pores and excellent chemical/thermal stability. Various organic and inorganic nanotube structures have been successfully fabricated by AAO-assisted template approach [8–11]. However, the production yield of this synthesis approach is critically limited by the total area of the AAO template and the time-consuming template fabrication process itself. The most widely used fabrication method of AAO is the so-called mild anodization (MA), which usually takes more than one day to get ordered nanoporous structure with limited self-ordering windows [12]. To achieve simple and fast fabrication of AAO with wide range of pore size, an industrialized anodization technique so-called hard anodization (HA) has been recently utilized in nanotechnology to get high aspect ratio AAO nanostructures within a short time [13,14]. However, HA process is relatively less stable as compared to MA process mainly due to the extensive heat generation as high voltage or current are required.

To overcome these limitations and to fabricate novel nanotube structures from AAO templates, recently Lee et al. developed a facile route for fabricating anodic alumina nanotubes (AANTs) by pulse anodization (PA) [15]. This method significantly improved the yield of nanotube production by creating stack-layered AAO structures during PA and subsequently breaking down the pulse-anodized AAO into individual AANTs under precisely designed condition. Although large quantities of nanotube can be fabricated by this electrochemical approach, the detailed formation mechanism of AANTs has not been exhaustively investigated yet. A better understanding of the generation

* Corresponding author.
E-mail addresses: abel.santos@adelaide.edu.au (A. Santos), andreas.evdokiou@adelaide.edu (A. Evdokiou), dusan.losic@adelaide.edu.au (D. Losic).

http://dx.doi.org/10.1016/j.electacta.2014.12.056
0013-4686/

mechanism of AANTs would enable better control over the dimensions, morphology and geometric features of this novel one-dimensional nanomaterial. AANTs have unique hollow lumen structure and stable physiochemical properties, which have great potential to be used as templates for nano-fabrication or directly be used as nanocontainer for advanced applications such as drug delivery. Our recent work also demonstrated that as-prepared AANTs with average length 600 nm have excellent biocompatibility and can efficiently deliver high amount of therapeutic drugs for potential cancer therapy [16].

In this article, we report for the first time on the synthesis of ultra-short AANTs by a rationally designed short-time PA. The fabrication of short AANTs (i.e. length < 600 nm) is important to reduce their cytotoxicity given that the reduced length can improve macrophage clearance and reduce intracellular stress [17,18]. A precise control over the AANTs dimensions and geometry can also provide a versatile platform for other advanced applications such as template-assisted nanofabrication. However, the fabrication of ultra-short AANTs has not been achieved yet due to the lack of understanding of this fabrication process. To shed light on this gap, we systematically investigated the impact of the starting layer thickness, the current density, the pulse duration and the electrolyte composition during AANTs fabrication (Scheme 1). The understanding of the intrinsic formation mechanism of AANTs not only provides us a new insight to structurally engineer AAO by PA, but also makes it possible to successfully reduce the resulting length of AANTs down to 485 nm, which is not achievable by the existing nanofabrication methods.

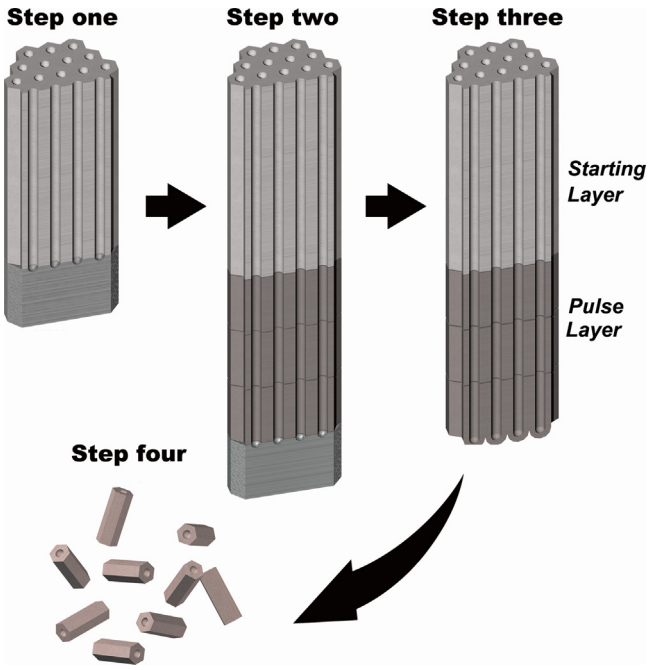

Scheme 1. Schematic illustration of the fabrication process of AANTs by galvanostatic pulse anodization. Electrochemically polished aluminum was first anodized at MA conditions to grow a certain thickness of oxide layer (starting layer). Afterwards, galvanostatic pulse anodization was performed by applying a series of current density pulses to switch the anodization regime between MA and HA conditions. Finally, the remaining aluminum substrate was removed by selective acid etching and liberated AANTs were obtained by acid etching and gentle sonication.

2. Experimental

2.1. Materials and chemicals

Aluminum (Al) foils of thickness 0.32 mm and purity 99.9997% were supplied by Goodfellow Cambridge Ltd. (UK). Sulfuric acid (H_2SO_4), copper(II) chloride ($CuCl_2$), hydrochloric acid (HCl), ethanol (denatured) (C_2H_5OH), perchloric acid ($HClO_4$), chromium trioxide (CrO_3) and phosphoric acid (H_3PO_4) were purchased from Sigma-Aldrich (Australia) and used without further processing. Ultrapure water Option Q–Purelabs (Australia) was used for preparing all the solutions used in this study.

2.2. Fabrication of anodic alumina nanotubes by pulse anodization

AANTs were synthesized by a modified pulse anodization process [15]. Briefly, Al chips 1.5 cm in diameter were first sonicated in ethanol and ultrapure water. Al chips were electro-polished prior to anodization in a mixture of ethanol and $HClO_4$ 4:1 (v:v) at 20 V and 5 °C for 3 min. After this, the first anodization step was carried out in an electrolyte of 0.3 M H_2SO_4 at 25 V and 6 °C for 5 h, 10 h, 15 h and 20 h to obtain starting layer thicknesses of 33 μm, 65 μm, 90 μm and 110 μm, respectively. Subsequently, pulse anodization was conducted under galvanostatic conditions at 1 °C with vigorous stirring. The area exposed to the electrolyte solution was 0.95 cm^2 and the current density (j) calculated by dividing the input current by the anodized sample area. This anodization step consisted of a periodic combination of MA and HA pulses in 0.3 M H_2SO_4 electrolyte, which was modified with various concentrations of ethanol ranging from 0% to 25%. After that, the remaining aluminum substrate was removed by wet chemical etching in a mixture of 0.2 M $CuCl_2$ and 6.1 M HCl. Free-standing AANTs were obtained by immersion in the same acid solution for 5 to 30 mins at room temperature followed by gentle ultrasonic treatment for one hour.

2.3. Structural characterizations

The shape and structure of prepared AANTs and pulse-anodized AAO structure were characterized by a transmission electron microscope (FEI Tecnai G2 Spirit TEM) and a field emission gun scanning electron microscope (FEG-SEM FEI Quanta 450). The size distribution of AANTs was calculated by counting approximately 500 AANTs from three independent experiments and their geometric features (i.e. length and inner and outer diameters) established by image analysis using ImageJ software.

3. Result and discussion

3.1. The thickness of starting layer influences the structural modulation of the outer wall of nanopores

Self-ordered AAO films were traditionally fabricated by MA process, in which a slow oxide growth rate (i.e. 2–7 μm/h) is achieved under low current density ($j = 1–5$ mA/cm^2) conditions [12]. In contrast, HA conditions at high current density (i.e. $j > 30$ mA/cm^2) made it possible to produce self-ordered AAO films at high growth rates (i.e. 40–60 μm/h) [13]. Unlike conventional MA process, an oxide layer must be formed on the surface of the aluminum substrate before HA process to suppress breakdown effects, avoid plastic deformation, achieve self-organization and improve the mechanical integrity of the resulting AAO film. For the same reason, a protective oxide layer (i.e. starting layer) is necessary before galvanostatic PA is started due to the high current density at HA condition.

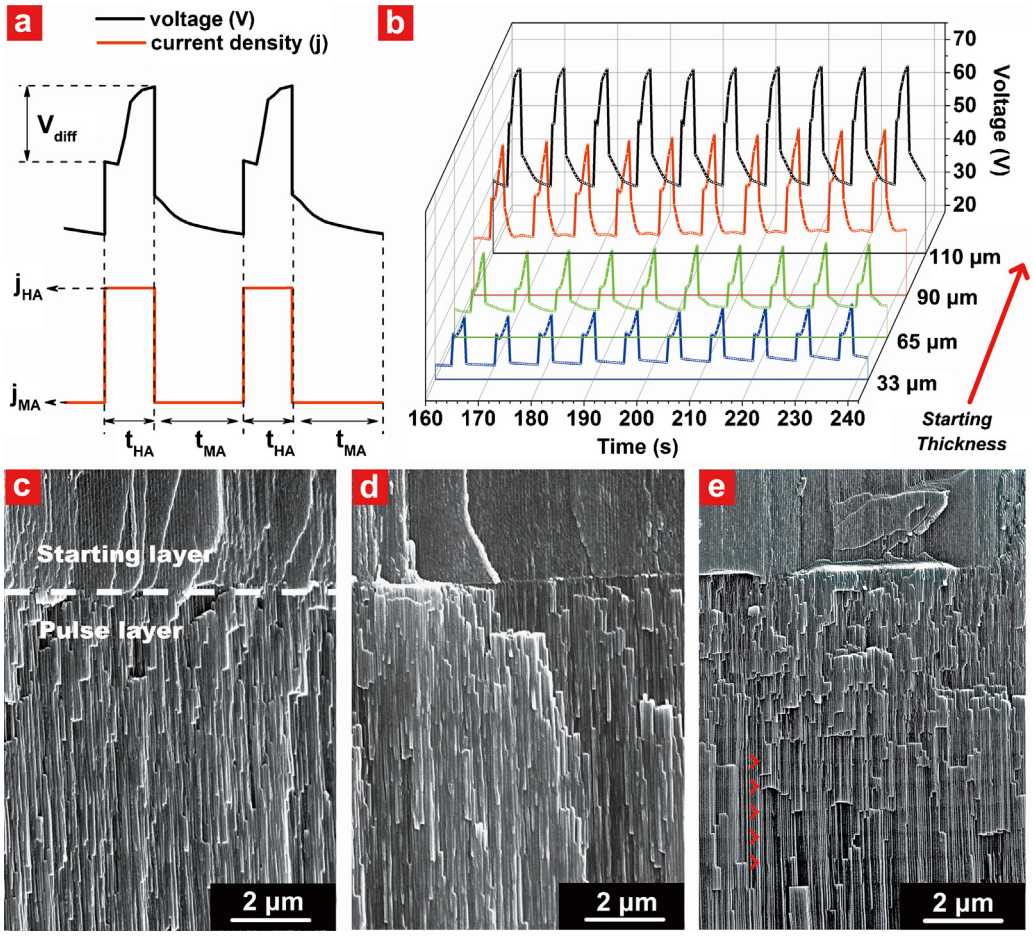

Fig. 1. The fabrication of stack-layer nanostructure by pulse anodization is depend on the starting thickness of AAO. (a) Scheme of HA/MA pulse used for pulse anodization. j_{HA}/j_{MA} is the current density applied to achieve HA/MA conditions; t_{HA}/t_{MA} is pulse durations, and V_{diff} denotes the anodization voltage difference between the starting and ending stage of each HA-pulse. (b) Representative voltage-time profile of pulse anodization with different starting layer thickness. The anodization condition was maintained at j_{MA} = 3.26 mA/cm^2/t_{MA} = 5 s and j_{HA} = 368.52 mA/cm^2 and t_{HA} = 2 s. (c–e) Cross-section SEM images of AAO nanostructure with starting layer thickness of 33 μm (c), 65 μm (d) and 110 μm (e). White dash line indicates the interface formed by the transition from MA to HA. Red arrow heads showed the resulting spaced layer structure.

Strikingly, we found that the starting layer thickness directly influences the structural modulation of the outer wall of nanopores during PA (Fig. 1). To study the impact of the starting layer thickness, we first conducted potentiostatic MA instead of HA in order to have a better control over the starting layer thickness. The next step of PA pulses consisted of 30 cycles of current pulses. Each pulse constitutes a HA-pulse followed by a MA pulse as illustrated in Fig. 1a. The voltage-time profiles in Fig.1b clearly showed thickness-dependent voltage recovery effect, where the value of the voltage difference between the starting and ending stage of each HA-pulse (V_{diff}) gradually increased with the starting layer thickness from approximately 5 V at 33 μm to 17 V at 110 μm. Correspondingly, the resulting pulse-anodized AAO nanostructure with starting layer thicknesses of 33 μm and 65 μm did not show significant outer wall modulation, although the space-layered nanostructure could be recognized (Fig. 1c and d); the structural modulation become evident with the starting layer thickness of 110 μm, as shown in Fig. 1e. This structural modulation pattern can directly influence the AANTs fabrication: AANTs can only be obtained from AAO structure with starting layer thickness of 110 μm after acid etching and sonication treatment (Fig. S 1 supporting information).

From these results, we infer that the generation of extensive Joule's heat at the nanopore's bottom during PA might contribute to this thickness-dependent voltage recovery pattern. According to Joule's law of heat, the Joule's heat (Q) at a given time (t) can be expressed as:

$$Q = Rj^2t \quad (1)$$

where R is the electronic resistance of the barrier layer and j is the applied current density. HA conducted at high current density is accompanied by a large evolution of heat as compared to MA. The extensive heat generation can cause the dissolution of aluminum oxide in the acid electrolyte and thus enhance the ionic flow across the oxide barrier layer at the pore bottom, which will eventually lead to electric breakdown [19,20]. Pulse anodization is an effective method to dissipate the Joule's heat by introducing a MA step after HA [21–23]. However, with the increasing thickness of the starting layer, the convective heat transfer in the electrolyte might not be efficient enough to dissipate the generated heat due to the confinement of long-ranged nanopores. Such heat generation at the nanopore bottom can unavoidably lead to the partial dissolution of the oxide barrier layer, thus facilitating the rapid voltage recovery.

Note that so far there is no direct method to measure the *in situ* Joule's heat generation at the nanopore bottom. To verify our hypothesis about the role of heat evolution on AANTs' fabrication, we lowered the HA current density down to 210.52 mA/cm^2 to reduce the heat generation during HA pulse while maintaining the starting layer thickness at 110 μm. Interestingly, no AANTs were obtained within 2 s HA pulse, while AANTs can be readily fabricated by extending HA duration to 10 s. The anodization

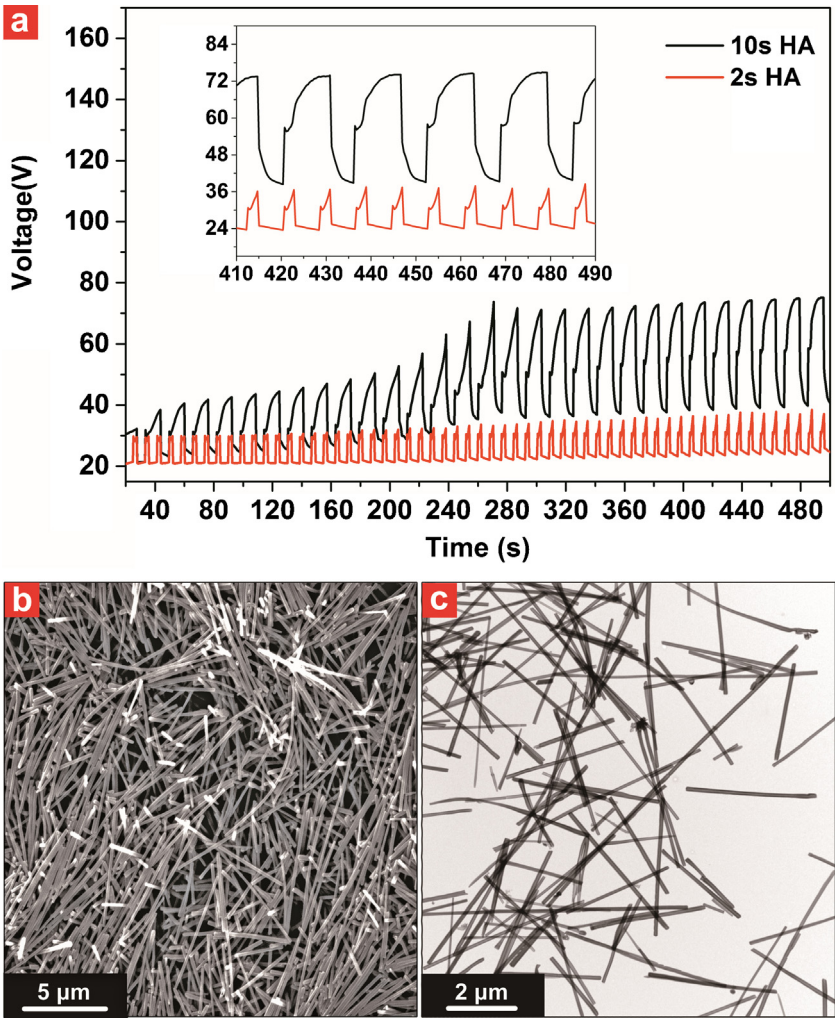

Fig. 2. The effect of reduced current density and extended HA pulse duration on the AANTs fabrication. (a) Representative voltage-time profile at j_{HA} = 210.52 mA/cm^2 and starting layer thickness of 110 μm. HA duration was set to 2 s and 10 s, respectively, followed by 5 s MA pulse at j_{MA} = 3.26 mA/cm^2. A magnified voltage-time profile at the late stage of anodization is shown in the inset. (b) TEM and (c) SEM characterization of AANTs fabricated by 10 s HA with j_{HA} = 210.52 mA/cm^2.

profile in Fig. 2a showed that the reduction of current density significantly retarded the voltage recovery pattern within 2 s HA pulse, which is similar to the pattern of 33 μm and 65 μm starting thicknesses at j_{HA} = 368.52 mA/cm^2. Extending HA duration to 10 s showed a complete voltage recovery pattern with a HA potential difference of approximately 17 V at the late stage of the PA process. In addition, voltage gradually increased with the anodization time during this process and stabilized at 74 V. However, the maximum voltage of 2 s HA pulse did not increase significantly after a number of pulse cycles. This voltage-time pattern strongly indicated that the continuous heat generation during 10 s HA pulse contributes to the sufficient voltage recovery pattern as well as the increasing of anodization voltage to a maximum value. The Joule's heat evolution was significantly reduced at j_{HA} = 210.52 mA/cm^2 as compared to the case of j_{HA} = 368.52 mA/cm^2. Therefore, the generated Joule's heat during a 2 s HA pulse can be efficiently dissipated by the following 5 s MA pulse, which lead to a relative stable anodization voltage at a low value as well as the retarded voltage recovery pattern. Nevertheless, this drawback can be overcome by extending the duration of HA pulse to achieve sufficient voltage recovery and consequently to trigger the modulation of the wall structure (Fig. S 2 supporting information). As a result, AANTs with average length 3.64 ± 1.53 μm can be obtained at the condition of 10 s HA pulse with j_{HA} = 210.52 mA/cm^2 (Fig. 2b and c), while no AANTs was produced under the 2 s HA pulse at j_{HA} = 210.52 mA/cm^2.

3.2. Sufficient oxygen evolution is required for AANTs liberation

The fabrication of AANTs from pulse-anodized AAO film requires the cleavage of the AAO nanostructure at the conjunction of layers as well as between the cell boundaries. Therefore, understanding the mechanism of cell separation effect is of critical importance to improve the liberation of AANTs from pulse anodized AAO films. To characterize the inner porous structure, we prepared microtome sections of pulse anodized AAO nanostructure. As shown in Fig. 3a, a clearly modulation of inner pore structure was observed at the interface of each layer, which is created by the transition of current density between HA and MA regime [22,24]. While the inner diameter of nanopores at the modulation point (i.e. transition between MA and HA pulse) is 8.5 ± 1.8 nm, it becomes 24.5 ± 4.8 nm during the HA pulse. Note that the areas between two adjacent cells appeared to be brighter than the nanopore's wall structure in TEM, indicating the existence of material with less atomic density along cell boundaries (Fig. 3b and c). The generation of gas voids and aluminum hydroxide has long been considered as the main cause of cell separation effect at HA performed under high current density or voltage conditions

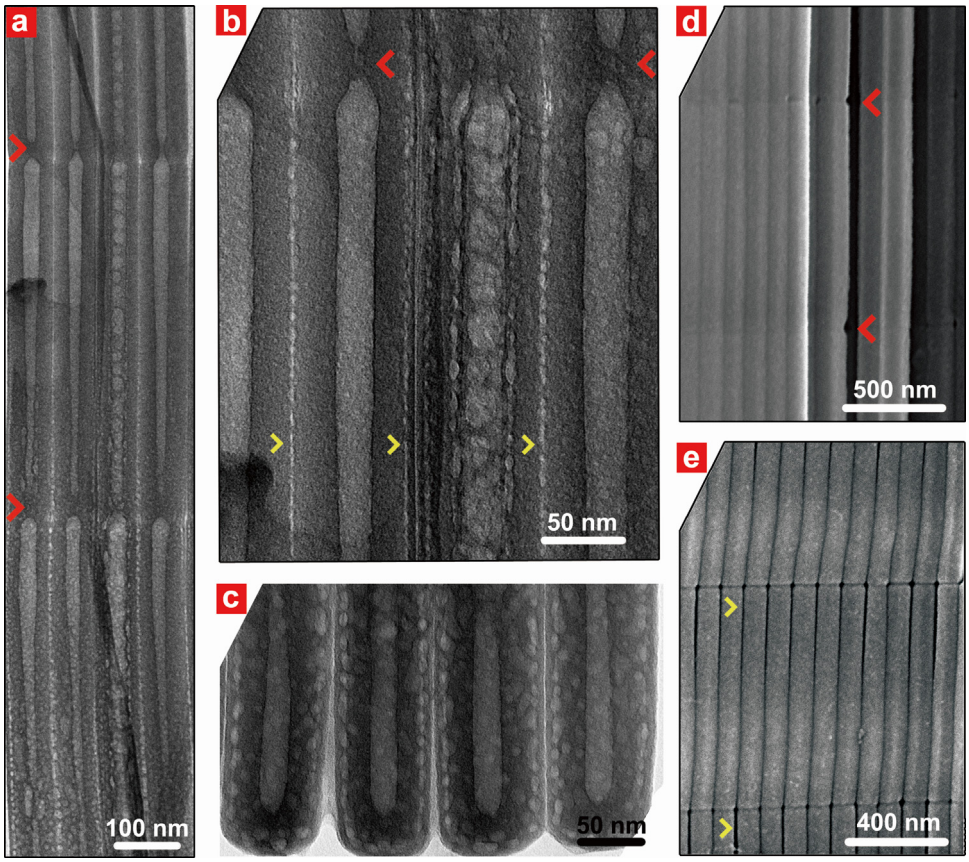

Fig. 3. Evidence of oxygen evolution during pulse anodization. (a-c) TEM characterization of resulting AAO nanostructure fabricated by pulse anodization at the condition of j_{MA} = 3.26 mA/cm^2/t_{MA} = 5 s and j_{HA} = 368.52 mA/cm^2 and t_{HA} = 2 s. The cross section image (a) and the bottom image (c) clearly show air voids along the cell boundaries. A magnified cross-section image is shown in (b). (d and e) SEM images of AAO nanostructure before (d) and after (e) acid etching. Red arrow heads show the modulation of the nanoporous structure. Yellow arrow heads show the voids and gaps along the cell boundaries.

[25–27]. We hereby assumed that the compositions of bright layers are possibly aluminum hydroxide and voids generated by the oxygen evolution during PA process. After immersing the AAO film in HCl/$CuCl_2$ solution for a short time, a clear gap along adjacent cell boundaries can be observed, indicating the dissolution of aluminum hydroxide after acid etching (Fig. 3d and e). Therefore, our results are in good agreement with previously published studies, confirming that the generation of aluminum hydroxide and oxygen bubbles along cell boundaries are critical to induce the cell separation during pulse anodization. Since the electrochemical reaction of oxygen evolution is controlled by the current density, it is expected that HA pulses with high current density would produce cell separation effect more efficiently than low HA current density pulses.

3.3. Fabrication of ultra-short AANTs by modifying electrolyte

Fabricating ultra-short AANTs is of great interest to improve their future application such as drug delivery. We attempted to reduce HA pulse duration to shorten the resulting length of AANT. However, the resulting voltage-time pattern showed an incomplete voltage recovery during short-time PA, which led to the failure of AANTs production (Fig. 4a). As shown in the above sections, the fabrication of AANTs is controlled by current density, HA duration and heat generation during PA. Although reduced HA duration can shorten the resulting thickness of HA layer section at a given current intensity, it unavoidably leds to a reduced heat generation during HA, which is unfavorable for AANTs fabrication. Therefore, other strategies need to be established to maintain the heat generation during short time PA.

We found that adding certain amount of ethanol (EtOH) (5–10%v) is necessary for obtaining liberated AANTs when short-time HA pulses are used. Fig. 4a shows the representative current-voltage profiles with 1 s HA pulse at j_{HA} = 368.52 mA/cm^2. The addition of 10% EtOH to the electrolyte can generate efficient voltage recovery within 1 second HA pulse as compared to the PA with 0.3 M H_2SO_4. The resulting pulse-anodized AAO clearly showed spaced-layer structure with approximately 500 nm thickness (Fig. 4b). After liberation, AANTs with average length 485 ± 180 nm can be obtained (Fig. 4c and d). Note that the average inner wall diameter is 33.0 ± 8.0 nm, which is slightly bigger than that of the pore diameter before liberation. This can be associated to acid dissolution effect during the liberation process.

We assume that EtOH can promote heat generation during short-time PA, which facilitated the liberation of AANTs from pulse-anodized AAO nanostructure. To understand the function of ethanol during short-time PA, we performed galvanostatic HA at j_{HA} = 368.52 mA/cm^2 with a starting layer thickness of 110 μm (Fig. 5). HA in 0.3 M H_2SO_4 showed a typical voltage profile characteristic of galvanostatic anodization [1]. Voltage reaches a maximum value during the initial stage of this process and becomes stable at appromixtely 69 V. Then, after this initial stage, voltage increases gradually due to the intensive Joule's heat generation during HA. Finally, the local breakdown of the AAO film takes place after 16 mins, which is characterized by the abrupt increament of the anodization voltage. Note that we observed plastic deformation and non-uniform thickness distribution of the anodic film after long time HA, which is caused by uneven-distributed heat generation and current flow at the pore bottom (Fig. S 3 supporting information) [19,20]. In contrast, when HA was

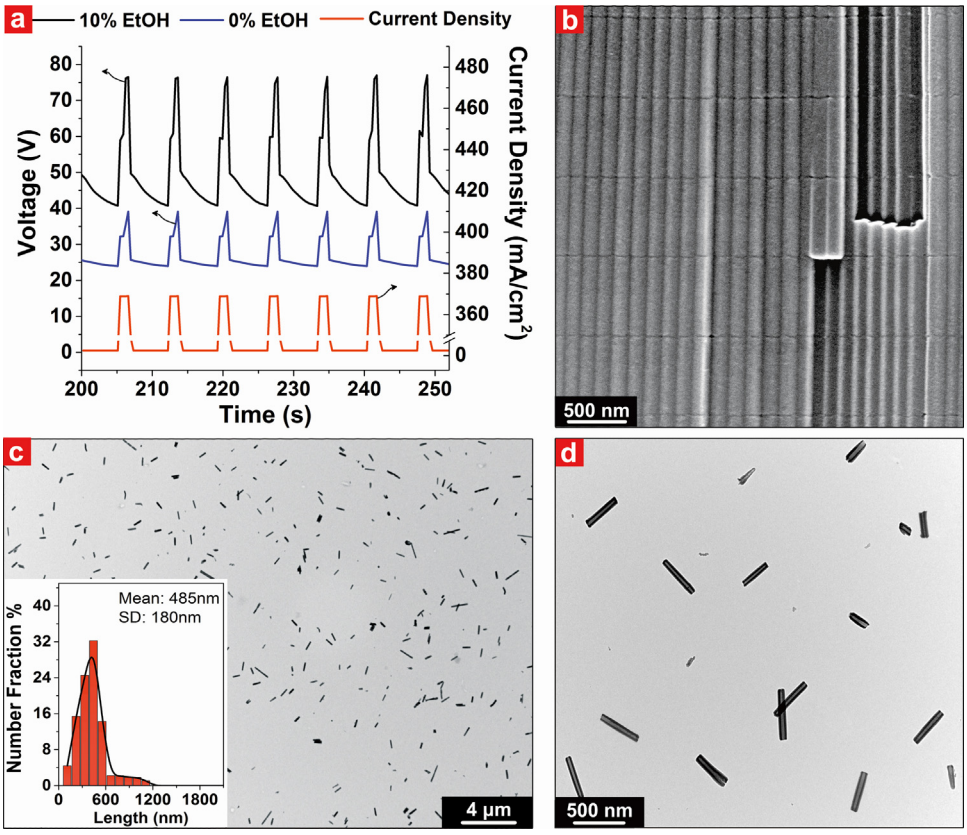

Fig. 4. Fabrication of ultra-short AANTs by manipulating electrolyte composition. (a) A representative voltage-current anodization profile under the condition of 1 s HA pulse. The electrolyte with 0.3 M H_2SO_4 did not create rapid voltage recovery. The addition of 10% ethanol can efficiently induce around 17 V voltage difference during 1 s HA pulse (b) SEM cross-section view of the AAO nanostructure fabricated by the condition of 1 s HA pulse. (c and d) TEM characterization and size distribution of resulting ultra-short AANTs.

performed in EtOH-modified H_2SO_4 electrolyte, a significant faster breakdown pattern was observed as compared to the electrolyte system without ethanol. HA with 5%v EtOH showed steady porous growth pattern at the beginning, but electric breakdown happened after 362 ± 10 s. HA with 10%v EtOH showed a rapid breakdown pattern after 130 ± 20 s. Furthemore, we found out that the breakdown effect can happen in a few seconds when the concentration of EtOH is increased up to 20%v. From these results we hypothesize that the ethanol concentration-dependant breakdown effect is caused by the rapid heat generation at the bottom of the nanopores, which leads to the catastrophic local flow of current across the oxide barrier layer. EtOH has been frequently used as a coolant to achieve HA condition under high electric field conditions at temperatures below 0 °C [28–30]. However, our result demonstrated that EtOH is not efficient to dissipate the heat generated during HA process when the temperature of the electrolyte is relatively high. The rapid heat generation at the bottom of the nanopores, however, can be efficiently dissipated by PA, and thus a steady growth of the anodic film can be achieved. As discussed above, the voltage recovery rate during HA is directly associated with localized heat generation. Therefore, the rapid heat generation in EtOH-modified electrolyte contributed to the fast voltage recovery within a short-time HA pulse (1 s), which generated sufficient structural modulation and cell separation for successful AANT liberation.

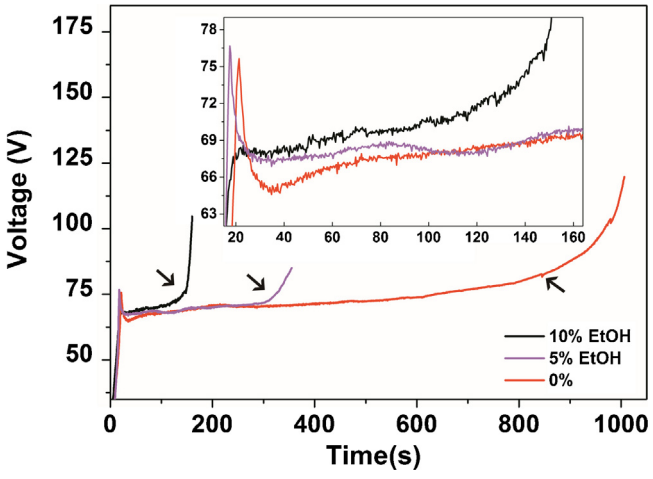

Fig. 5. HA anodization profile with ethanol-modified electrolyte. AAO film with starting layer thickness of 110 μm was directly anodized at a constant current density of 368.52 mA/cm^2. Ethanol addition can significantly shorten the breakdown time. Black arrows indicate the breakdown time point for each percentage of ethanol. Insert depicts an enlarged voltage-time profile of HA during the anodization time between 20 s to 160 s.

We also found that as-prepared ultra-short AANTs have a unique narrow ending at one side (Fig. 6c). This structure is engineered by switching the current density between HA and MA regimes, as illustrated in Fig. 3. Nonetheless, AANTs should have narrow structures on both ends if nanotubes were evenly cleaved at the site of structural modulation of outer wall. To investigate the liberation mechanism of AANTs, we performed SEM characterization of the pulse-anodized AAO nanostructures after extensive acid etching. It is evident that the connection between layers were completely removed and the nanotubes started to detach from the AAO film after long time etching (Fig. 6a). At higher magnification,

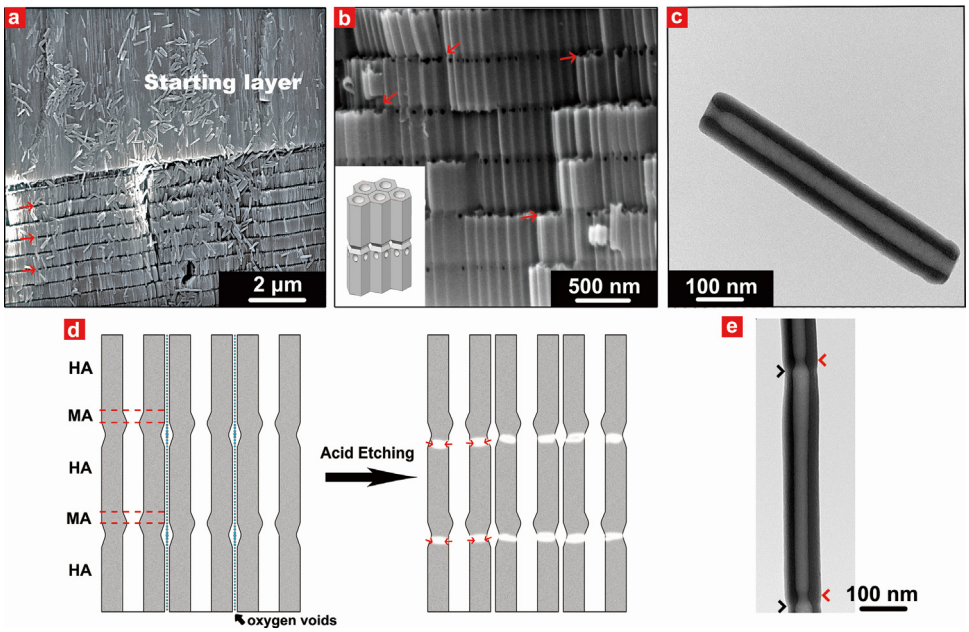

Fig. 6. Effect of chemical etching of pulse-anodized AAO structure on AANTs liberation. (a) A SEM cross-section image and schematic (bottom inset) of pulse anodized AAO structure after extensive acid etching. The anodization condition was $j_{MA} = 3.26\ mA/cm^2/t_{MA} = 5s$ and $j_{HA} = 368.52\ mA/cm^2/t_{HA} = 1s$. (b) A representative magnified SEM cross-section image showed that periodically perforated pores appeared at the region close to the modulated wall structure, which corresponded to the starting stage of HA pulse. Red arrows show the cleavage of AANTs after etching. (c) A representative TEM image of single a AANTs, showing a unique narrow ending structure at one side of the nanotubes. (d) Schematic illustration of chemical etching process. The asynchronous inner/outer wall structural modulation generates a weak conjunction along the interface of HA/MA segment, which can be preferably removed after acid etching. (e) TEM characterization of a single liberated AANTs with joint connection. The back/red arrow heads show outer/inner wall modulation respectively.

periodically perforated pores can be seen at the area close to the modulated wall structure, which corresponds to the starting stage of HA pulse (Fig. 6b). The formation of perforated pores is due to the selective chemical dissolution at the position where the thickness of the pore wall structure is the thinnest [31]. As discussed above, the modulation of the inner pore diameter happened at the time point when current density was switched between HA and MA regimes [22,24], while the outer pore modulation was engineered by the voltage recovery effect at the beginning of HA pulse. Therefore, the structural modulation of outer pore wall should happen after the inner wall modulation, which created a thinner wall structure as compared to the HA-segment and MA-segment (Fig. 6d). This thin layer can be etched faster than other area, and thus created the perforated pores and weakness conjunction along the interface of HA-MA segment. This liberation mechanism is well supported by the finding that AANTs with joint connections have asynchronous inner/outer wall structural modulation (Fig. 6e). The elucidation of AANTs' liberation mechanism is of fundamental importance for AANTs fabrication. It can be expected that more sophisticated AANTs structure can be fabricated by using PA to engineer inner pore geometry and simultaneously generate structural modulation of outer pore for AANTs liberation.

4. Conclusion

In summary, we have reported an innovative approach for fabricating ultra-short AANTs by galvanostatic PA. Out results proved that the heat generation plays a key role for AANTs fabrication. Sufficient heat generation at the pore bottom is necessary to achieve the rapid voltage recovery and oxygen evolution for creating weakened conjunctions along cell boundaries as well as along MA/HA interfaces. We have demonstrated that creating the starting porous layer with specific thickness (110 μm) and manipulating the electrolyte composition with EtOH are essential factors to produce ultra-short AANT under short-time PA. These findings not only improve our understanding of PA of aluminum, but also provide a facile, comprehensive and cost-competitive method to fabricate large quantities of well-defined ultra-short AANTs nanostructures with average length 485 ± 180 nm. These nanostructures afford great opportunities in a broad field of applications such as catalysis, sensing, template-assisted nanofabrication, energy storage and drug delivery due to their unique hollow nanostructure and superior thermal/biological stability.

ACKNOWLEDGMENTS

This research was supported by the Australian Research Council (ARC) and the National Health and Medical Research Council (NHMRC) through the grants DP120101680,FT110100711, DE14010054 and APP627015. Authors thank Mr. Jason Peak, Mr. Michael Jung and Mr. Jeffrey Hiorns from the mechanical workshop for their help and support with the fabrication of the experimental set-ups used in this study. Authors appreciate the Adelaide Microscopy (AM) centre for FEG-SEM and TEM characterization. Ye Wang appreciate the scholarship support from China Scholarship Council.

Appendix A. Supplementary data

Supplementary data associated with this article can be found, in the online version, at http://dx.doi.org/10.1016/j.electacta.2014.12.056.

References

[1] W. Lee, S.-J. Park, Porous Anodic Aluminum Oxide: Anodization and Templated Synthesis of Functional Nanostructures, Chem.Rev. 114 (15) (2014) 7487–7556.
[2] A.M. Jani, D. Losic, N.H. Voelcker, Nanoporous anodic aluminium oxide: Advances in surface engineering and emerging applications, Prog. Mater. Sci. 58 (5) (2013) 636–704.

[3] A. Santos, M.S. Aw, M. Bariana, T. Kumeria, Y. Wang, D. Losic, Drug-releasing implants: current progress, challenges and perspectives, J. Mater. Chem. B 2 (2014) 6157–6182.
[4] T. Kumeria, M.M. Rahman, A. Santos, J. Ferré-Borrull, L.F. Marsal, D. Losic, Nanoporous Anodic Alumina Rugate Filters for Sensing of Ionic Mercury: Toward Environmental Point-of-Analysis Systems, ACS Appl. Mater. Interfaces 6 (2014) 12971–12978.
[5] P. Banerjee, I. Perez, L. Henn-Lecordier, S.B. Lee, G.W. Rubloff, Nanotubular metal-insulator-metal capacitor arrays for energy storage, Nat Nano 4 (2009) 292–296.
[6] G.D. Sulka, K. Hnida, A. Brzózka, pH sensors based on polypyrrole nanowire arrays, Electrochim. Acta 104 (2013) 536–541.
[7] Y. Liu, J. Goebl, Y. Yin, Templated synthesis of nanostructured materials, Chem. Soc. Rev 42 (2013) 2610–2653.
[8] G.D. Sulka, A. Brzózka, L. Liu, Fabrication of diameter-modulated and ultrathin porous nanowires in anodic aluminum oxide templates, Electrochim. Acta 56 (2011) 4972–4979.
[9] J. Martín, M. Martín-González, J. Francisco Fernández, O. Caballero-Calero, Ordered three-dimensional interconnected nanoarchitectures in anodic porous alumina, Nat Commun 5 (2014) , doi:http://dx.doi.org/10.1038/ncomms6130.
[10] H. Masuda, K. Fukuda, Ordered Metal Nanohole Arrays Made By a 2-Step Replication Of Honeycomb Structures Of Anodic Alumina, Science 268 (5216) (1995) 1466–1468.
[11] G. Meng, Y.J. Jung, A. Cao, R. Vajtai, P.M. Ajayan, Controlled fabrication of hierarchically branched nanopores, nanotubes, and nanowires, Proc. Natl. Acad. Sci. U. S. A. 102 (20) (2005) 7074–7078.
[12] K. Nielsch, J. Choi, K. Schwirn, R.B. Wehrspohn, U. Gösele, Self-ordering Regimes of Porous Alumina: The 10 Porosity Rule, Nano Lett. 2 (2002) 677–680.
[13] W. Lee, R. Ji, U. Gosele, K. Nielsch, Fast fabrication of long-range ordered porous alumina membranes by hard anodization, Nat Mater 5 (2006) 741–747.
[14] A. Santos, J.M. Montero-Moreno, J. Bachmann, K. Nielsch, P. Formenti'n, J. Ferre'-Borrull, J. Pallarès, W.L.s.F Marsal, Understanding Pore Rearrangement during Mild to Hard Transition in Bilayered Porous Anodic Alumina Membranes, ACS Appl. Mater. Interfaces 3 (2011) 1925–1932.
[15] W. Lee, R. Scholz, U. Gösele, Nano Letters, A Continuous Process for Structurally Well-Defined Al_2O_3 Nanotubes Based on Pulse Anodization of Aluminum, Nano Lett. 8 (2008) 2155–2160.
[16] Y. Wang, A. Santos, G. Kaur, A. Evdokiou, D. Losic, Structurally engineered anodic alumina nanotubes as nano-carriers for delivery of anticancer therapeutics, Biomaterials 35 (2014) 5517–5526.
[17] A.E. Nel, L. Madler, D. Velegol, T. Xia, E.M.V. Hoek, P. Somasundaran, F. Klaessig, V. Castranova, M. Thompson, Understanding biophysicochemical interactions at the nano-bio interface, Nat Mater 8 (2009) 543–557.
[18] K. Kostarelos, The long and short of carbon nanotube toxicity, Nat Biotech 26 (2008) 774–776.
[19] S. Tajima, Luminescence: breakdown and colouring of anodic oxide films on aluminium, Electrochim. Acta 22 (1977) 995–1011.
[20] J.M. Albella, I. Montero, J.M. Martinez-Duart, A theory of avalanche breakdown during anodic oxidation, Electrochim. Acta 32 (1987) 255–258.
[21] W. Lee, K. Schwirn, M. Steinhart, E. Pippel, R. Scholz, U. Gosele, Structural engineering of nanoporous anodic aluminium oxide by pulse anodization of aluminium, Nat Nano 3 (2008) 234–239.
[22] L. Woo, K. Jae-Cheon, Highly ordered porous alumina with tailor-made pore structures fabricated by pulse anodization, Nanotechnology 21 (2010) 485304.
[23] C.K. Chung, W.T. Chang, M.W. Liao, H.C. Chang, C.T. Lee, Fabrication of enhanced anodic aluminum oxide performance at room temperatures using hybrid pulse anodization with effective cooling, Electrochim. Acta 56 (2011) 6489–6497.
[24] W. Lee, J.-C. Kim, U. Gösele, Spontaneous Current Oscillations during Hard Anodization of Aluminum under Potentiostatic Conditions, Adv. Funct. Mater. 20 (2010) 21–27.
[25] L. Yi, L. Zhiyuan, H. Xing, L. Yisen, C. Yi, Investigation of intrinsic mechanisms of aluminium anodization processes by analyzing the current density, RSC Adv. 2 (2012) 5164–5171.
[26] S.Z. Chu, K. Wada, S. Inoue, M. Isogai, A. Yasumori, Fabrication of Ideally Ordered Nanoporous Alumina Films and Integrated Alumina Nanotubule Arrays by High-Field Anodization, Adv. Mater. 17 (2005) 2115–2119.
[27] S. Zhao, K. Chan, A. Yelon, T. Veres, Novel Structure of AAO Film Fabricated by Constant Current Anodization, Adv. Mater. 19 (2007) 3004–3007.
[28] L. Yanbo, Z. Maojun, M. Li, S. Wenzhong, Fabrication of highly ordered nanoporous alumina films by stable high-field anodization, Nanotechnology 17 (2006) 5101.
[29] Y.B. Li, M.J. Zheng, L. Ma, High-speed growth and photoluminescence of porous anodic alumina films with controllable interpore distances over a large range, Appl. Phys. Lett. 91 (2007) 073109-073109-073103.
[30] L. Yi, L. Zhiyuan, C. Shuoshuo, H. Xing, H. Xinhua, Novel AAO films and hollow nanostructures fabricated by ultra-high voltage hard anodization, Chem. Commun. 46 (2010) 309–311.
[31] D. Losic, D. Losic, Preparation of Porous Anodic Alumina with Periodically Perforated Pores, Langmuir 25 (2009) 5426–5431.